View metadata, citation and similar papers at core.ac.uk

brought to you by CORE

provided by Biblioteca Digital da Produção Intelectual da Universidade de São Paulo (BDPI/USP)

Universidade de São Paulo

Biblioteca Digital da Produção Intelectual - BDPI

Departamento de Oceanografia Biológica - IO/IOB | Artigos e Materiais de Revistas Científicas - IO/IOB

2014

Mobility of meso-scale morphology on a microtidal ebb delta measured using remote sensing

Marine Geology, v. 357, p.334-343, 2014
http://www.producao.usp.br/handle/BDPI/48869

Downloaded from: Biblioteca Digital da Produção Intelectual - BDPI, Universidade de São Paulo

Marine Geology 357 (2014) 334–343

Contents lists available at ScienceDirect

Marine Geology

journal homepage: www.elsevier.com/locate/margeo

Mobility of meso-scale morphology on a microtidal ebb delta measured using remote sensing

Cassia Pianca [a,b,*], Rob Holman [b], Eduardo Siegle [a]

[a] IOUSP, Praça do Oceanográfico 191, University of São Paulo, São Paulo, SP 05508-120, Brazil
[b] 104, CEOAS Admin Bldg, Oregon State University, Corvallis, OR 97331, USA

ARTICLE INFO

Article history:
Received 6 March 2014
Received in revised form 20 September 2014
Accepted 24 September 2014
Available online 12 October 2014

Keywords:
ebb-tidal delta
meso-scale morphology
migration rates
rotational circulation
Argus video-images

ABSTRACT

Ebb tidal deltas usually consist of several large lobes of sediment separated by channels in which the bulk of the tidal exchange takes place. The purpose of this paper is to describe and quantify the migration pattern of bedform features associated with an ebb-tidal delta using a new remote video sensing method during a 23 day experiment at New River Inlet (North Carolina). To quantify the migration rates, a Lagged Least Squares Algorithm (LLSA) was developed that found the vector rate for which the suite of lagged images were most similar, computed on a tile-by-tile basis. Our observations revealed a complex set of bedform features that migrated in a circular pattern with movement in offshore regions being away from the inlet mouth and toward the shore while nearshore migration was back toward the inlet. 60% of the wavelength variability of these features is at scales that are smaller than the coherent channel and swash bar structures but much longer than megaripples, i.e., between 10 and 100 m. We have chosen to call these bedform features of meso-scale morphologies. The mean migration rate of these features was found to be 1.53 m/day ± 0.76 m/day. 72% of estimated rates were greater than 1.0 m/day, 31% were larger than 2.0 m/day, and the maximum rate was around 3.5 m/day, averaged over 23 days. Alongshore averages of cross-shore migration rates showed a node at 110 m from the shoreline that separates migration away from the inlet from migration toward the inlet (near the shore). The circular pattern of migration appeared to be consistent with expected residual flow of an ebb-tidal delta system.

© 2014 Elsevier B.V. All rights reserved.

1. Introduction

Tidal inlets are found along barrier coastlines throughout the world. They provide a passageway for ships and small boats to travel between the open ocean and sheltered waters so they are vital to a nation's commerce, recreation and safety.

Inlets are highly dynamic environments with their morphology governed by interactions between the tidal prism, waves versus tides energy and the local bathymetry. These inlets are normally associated with a main channel and tidal deltas on both the ebb (seaward) and flood (landward) ends of that channel. These sedimentary features have a strong influence in morphological changes of coastal regions, affecting the stability of the adjacent environmental, and contribute to the complex circulation patterns, leading to highly variable morphodynamic patterns (e.g. Komar, 1996; FitzGerald et al., 2000; Siegle et al., 2004, 2007; Son et al., 2010). It has been shown that the cross-sectional area of the main channel is determined by the back-bay tidal prism (O'brien, 1931; Stive and Rakhorst, 2008) and the relative balance of tidal prism and the longshore component of wave power appears to explain inlet stability (Bruun and Gerritsen, 1960). The dynamics of the tidal inlets and their associated sand bars structures are of great interest for the coastal sediment budget, coastline changes and the maintenance of navigation channels.

The morphology of ebb and flood deltas is principally a balance between deposition due to weakening currents as they spread away from the main channel and the potential for channelization caused by that deposition. However, this balance is altered by the role of wave-driven processes. When waves approach the shoreline, they refract over the shallow areas and wrap around the shoal margins. When they break, they create wave bores that travel shoreward and interact with tidal currents. This interaction may generate or enhance gyres that are dynamical sediment traps that cause accumulations of sand in the swash platforms (Oertel, 1972) or may recirculate back onto the ebb-tidal delta. Elias and Hansen (2013) in their study at the Golden Gate inlet, demonstrate through the application of a numerical model differences in the ebb delta hydrodynamic patterns due to waves. Their comparison of simulations with and without waves, clearly shows that waves interacting with the dominant ebb flow result in increased sediment movement across the ebb delta, following complex patterns such as a recirculation cell in one side of the inlet, while on the other side, the waves increase the seaward and longshore transport

* Corresponding author at: 104 CEOAS Admin Bldg, Oregon State University, Corvallis, OR, 97331, USA.
E-mail addresses: cpianca@coas.oregonstate.edu (C. Pianca), holman@coas.oregonstate.edu (R. Holman), esiegle@usp.br (E. Siegle).

http://dx.doi.org/10.1016/j.margeo.2014.09.045
0025-3227/© 2014 Elsevier B.V. All rights reserved.

Table 1
The table shows the wave statistics during the period of the experiment at NRI.

Wave parameter	Mean	Std
Hmo (m)	0.85	0.28
Tp (s)	6.48	1.70
Dir (deg)	141.12	29.00

onto and over the ebb-delta lobe platform. These effects can be due to the wave-driven current generated by the wave breaking over the shoals, and the wave-induced setup at the inlet mouth that exhibits a strong alongshore non-uniformity, resulting in a barotropic pressure gradient (Shi et al., 2011).

Circulation patterns at most of the tidal inlets are governed by a general trend of lateral segregation of the tidal currents. The deeper main channel is dominated by a strong outflow (ebb current), while the shallow and marginal regions of the inlet are dominated by the flood flow. This segregation is usually due to the time velocity asymmetry of the tidal currents (e.g. Hayes, 1975; FitzGerald et al., 2012). This asymmetry is attributed to the delay between the maximum velocities of flood and ebb currents, i.e., the maximum flood velocities usually occurring between mid and high-tide and the maximum ebb flow occurs between mid and low-tide, which in this case, due to the smaller water depths during low-tide result in flow constriction within the main channel. However, over the marginal shoals, the currents may not be associated entirely with ebb versus flood shifting tides. In some cases, the currents may be directed inward toward the inlet even when strong ebb flow is directed seaward along the main channel (e.g. Hayes et al., 1970; Dean and Walton, 1975).

Inlets probably represent one of the most challenging environments for the evaluation of sediment transport quantities related to the acting physical forces (Komar, 1996), and they have been the subject of a number of process-based models that provide valuable information on governing flow and sediment transport patterns (Wang et al., 1995; Cayocca, 2001; Ranasinghe and Pattiaratchi, 2003; Van Leeuwen et al., 2003; Siegle et al., 2004, 2007; Elias and Spek, 2006; Van der Vegt et al., 2006; Elias and Hansen, 2013). However, most of the previous studies have been focused on what might be called the macro-scale morphology of ebb shoals and channels, describing the ebb-tidal delta in terms of a small number of sediment lobes and channels. Little is known of the characteristics of smaller meso-scale morphology, features that are shorter than the coherent channel and bank structures but much longer than megaripples. The topography of these features is difficult to measure directly, but can be derived from remote sensing imagery (Woodroffe, 2002). A few, mostly recent, works have developed the idea of using video techniques to study morphological changes over the inlet channel (Morris et al., 2001; Medina et al., 2007), to extract shorelines of the major features around an estuarine region (Morris et al., 2007) and to study the evolution of the ebb-tidal delta morphologies (Balouin et al., 2004; Siegle et al., 2007). However, these studies have again focused mostly on the macro-scale morphology of the system. An early paper by Hine (1975) discussed the presence of shorter features pictured in an air photo (their Fig. 10) and measured in several survey transects but did not have temporal coverage to measure migration rates. While they used the term swash bars to describe these features, we will retain the term meso-scale morphologies since we are unclear of the role of swash in their formation, and most of the features are never exposed or at the swash zone, except the ones near the shoreline.

This paper will discuss recent observations of such meso-scale morphology observed using innovative optical methods and will document rates and patterns of migration of these features and their potential contribution to net sediment transport within the tidal delta complex. In the next section, we discuss the field area, the observational data for a May 2012 field experiment including a description of the Argus station that will form the basis for this study, then the development of a method for the robust estimation of migration rates from sequences of images collected over 23 days. The Results section will focus on documentation of the meso-scale features in Argus time exposure images and a comparison of these image features with survey ground truth data. This is followed by observations of a circular migration pattern, and quantification of the migration rates and pattern. We close with a discussion and conclusions.

2. Regional setting

The study area is located at New River Inlet (NRI) in North Carolina, US, between two barrier islands, North Topsail Beach to the west and Onslow Beach to the east (Fig. 1) and intersects the Intracoastal Waterway (around 3 km distance from the inlet mouth). North Topsail Beach is considered to be a high-risk zone (Cleary et al., 2006), particularly because of hurricanes and seasonal storms. New River is the largest fresh water source on Onslow Bay, with a drainage basin of 1240 km^2 (Cleary and Hosier, 1987). According to these authors, the NRI has

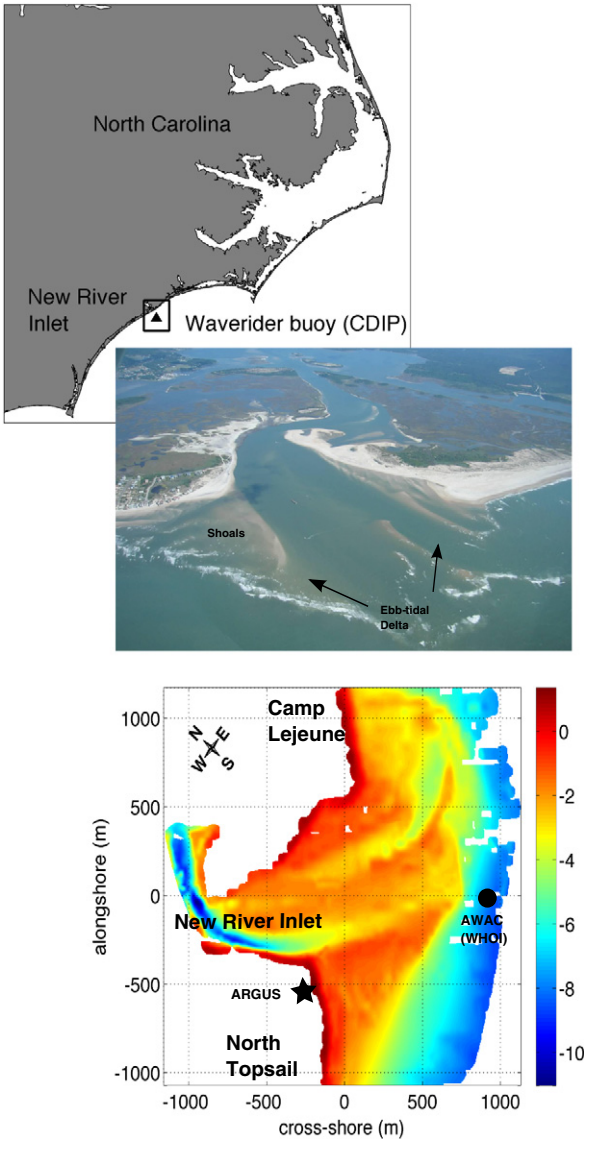

Fig. 1. Map and bathymetry of NRI. The aerial photo shows the position of the ebb shoals. The bathymetric map shows the Argus Station (black star) and the AWAC wave buoy from WHOI (black circle). The WaveRider buoy location from CDIP (Station #190) is represented with a black triangle on the top map.
The aerial photo was obtained from Gordon Farquharson (Applied Physics Laboratory — University of Washington).

been relatively unstable and migrating to the SW since the late nineteenth century, an average rate of 8.2 m/year. In 1986, the area of the ebb-tidal delta was estimated to be 830000 m^2 (Cleary and Hosier, 1987). The volume of the ebb-tidal delta was estimated to be 7 million m^3 out to a water depth of 6 m (Cleary et al., 2006).

The ebb-tidal delta extends seaward by around 1 km from the river mouth. The inlet currently has two channels, a deeper one (around 5 m deep) on the SW side of inlet and a secondary one (around 2 m deep) on the NE side of the inlet. The main channel is routinely dredged for shipping maintenance. Our observations revealed that the ebb shoals were composed of many bedform features that actively migrate in a clear pattern, which will be described in the following sections.

NRI is a micro-tidal region with semi-diurnal period. The shoreline is oriented NE and SW, thus it is exposed to waves propagating out of the ENE to SW. The freshwater discharge is minimal, and during the experiments the maximum discharge rates at peak ebb and flood were about 700 to 900 m/s, respectively (Wargula et al., 2013).

3. Observational data

3.1. Hydrodynamics data and bathymetry

The present work was part of a multi-institutional project called RIVET (RIVers and inlETs), an experiment to investigate the dynamics of a tidal inlet and the interactions between waves, currents and bathymetry over a complex ebb tidal shoal. The experiment took place from 26 April to 31 May of 2012.

Offshore water levels were measured using a bottom-mounted pressure sensor on a Nortek Acoustic Wave and Current Profiler (AWAC) moored in 9 meter water depth (34.52 N, 77.33 W), offshore of the ebb shoal (Fig. 2). The tide range varied from 1 to 2 m during the experiments. According to Lippman et al. (2013), tidal currents are semi-diurnal with maximum depth average speeds in the inlet of 1.5 m/s with an ebb dominance. Subtidal currents are typically driven by local winds in the offshore region, and can show a strong vertical variation that causes a complex 3D circulation in the inner shelf and can play a role in the net sediment transport in the region. Subtidal currents in the main channel (SW-side of the inlet) show reduced vertical structure and are directed seaward with strong flows. In the secondary channel the surface currents are directed landward and near-bottom currents are directed seaward. Wind speeds ranged from 0 to 14 m/s with directions from the NE or SW (Lippman et al., 2013; Wargula et al., 2013).

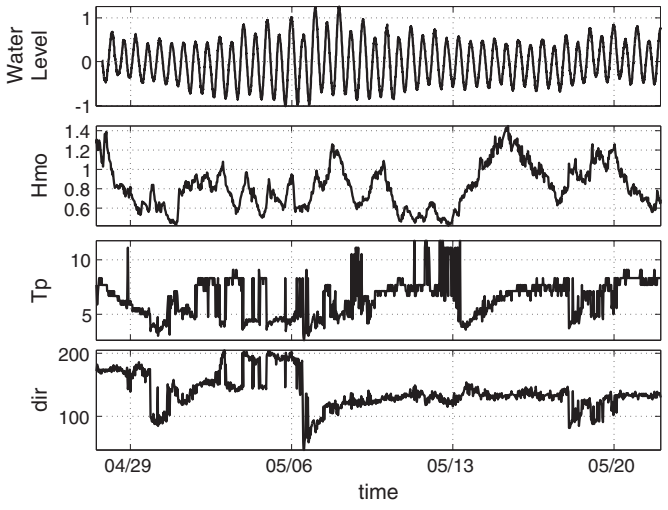

Fig. 2. Water level (m) obtained from the AWAC and time series of wave conditions: Hmo (m), Tp (s) and direction (degree) during the New Rivet experiments. The wave data were extracted from the waverider buoy at 13 m depth.

Wave conditions were measured every half hour for 1024 s at the AWAC sensor and also from a waverider buoy (CDIP Station # 190) located offshore in 13 m depth (34.48 N, 77.30 W) (Fig. 2). During the experiment the mean significant wave height ranged from 0.4 m to 2.5 m with one storm (2.5 m) and a few mild wave events (1.5 m to 2 m). Wave periods ranged from 4 to 9 s and wave directions varied primarily from S to E (See Table 1).

The bathymetry was surveyed 5 times (April 16–17, May 01–02, 10–11, 17–18 and 25 of 2012) during the experiment using the LARC-5 (Lighter Amphibious Resupply Cargo), which is an Army amphibious vehicle. The LARC is uniquely designed to allow surveying in the water, across shoals, and even through the surf zone up to the base of the beach dunes. More information about this vehicle can be obtained from http://www.frf.usace.army.mil/. 3D vehicle positional information was recorded frequently using a Trimble RTK-GPS survey system, accurate to approximately 5 cm. Depth below the vehicle was measured using a Knudsen 320B/P Echosounder. Data were recorded densely along-track but with a track spacing of 50 m in the alongshore direction. The resulting soundings were interpolated into 5 meter grid spacing and then were smoothed with a spatial function with a 25 m radius.

For convenience, an experiment coordinate system was designated with the origin in mid-channel (34.53 N, 77.34 W) and rotated 58° relative to true N to align with the mean shoreline. The +x is in the local offshore direction and +y is alongshore toward Cape Hatteras (NE).

3.2. Remote sensing Argus system

Optical sampling was carried out using six Argus video cameras mounted atop a tall retractable tower located in the driveway of rented house on the SW side of the inlet, 32 m above mean sea level. The combined views offer a roughly 200° field of view spanning from the beach (SW) into the inlet (E–NE). Five types of images were collected: snapshot, time exposure (Timex, averaging 2 Hz frames collected over a period of 10 min, Fig. 3), variance (standard deviation of same image series), brightest and darkest (the brightest and darkest intensities seen at each pixel during the ten-minute sample period (Holman and Stanley, 2007). The images were collected every half hour of daylight during the experiment.

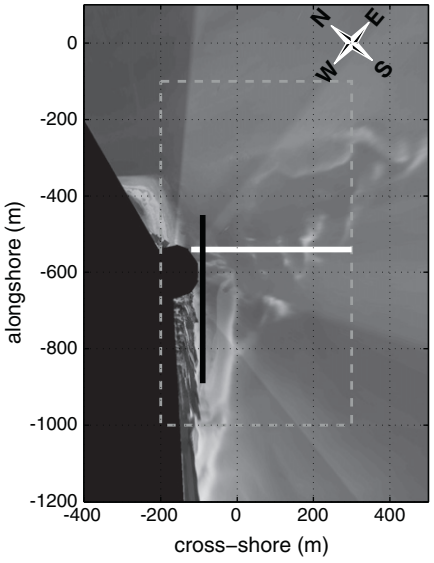

Fig. 3. Example of a merged geo-rectified time exposure image (timex) at the New River Inlet that combines the six camera views. White regions correspond to regions of enhanced breaking over shoals. The gray dashed box shows the region of interest for later analysis. The white line is an alongshore-oriented pixel transect at roughly x = −90 m while the black line is a cross-shore pixel transect at y = −540 m, respectively. Both were used to show below the presence of meso-scales variability in the area of interest and the magnitudes of dominant length scales.

A standard target was placed at a number of locations in the views of each camera and surveyed as temporary ground control points (GCPs). Camera viewing angles were found by comparing the image and survey locations using standard algorithms described in Holland et al. (1997). Possible changes in view, when the tower was lowered then raised again in response to thunderstorms or for camera maintenance, were tested for by regularly observing the image locations of a number of identifiable objects such as features on houses or an offshore piling. Camera motion was found to be negligible.

The pixel resolution is expressed in terms of the cross-shore and alongshore directions from each camera, where in the cross-range directions worsens with distance from the cameras while resolution in the range direction worsens in proportion to range squared. A region of interest between −800 m to −100 m (alongshore direction) and −200 m to 300 m (cross-shore direction) was defined for study of meso-scale features. Within this region the mean pixel resolution was 2 m in both the cross-shore and alongshore directions, with worst case resolutions of 3.5 m.

In 1989, time exposure imaging was introduced as a new method of visualizing and measuring nearshore morphology on an open beach (Lippmann and Holman, 1989). By averaging over shorter wave time scales, clutter was removed leaving an image showing patterns of enhanced wave dissipation that have been shown to correspond well to submerged sand bar or shoreline features (Lippmann and Holman, 1989; Holman et al., 1993; Lippmann et al., 1993; Holland et al., 1997; Holland, 1998; Van Enckevort and Ruessink, 2003a, 2003b; Plant et al., 2007; Pearre and Puleo, 2009). Since imaging is low cost and can span large areas, time exposure imaging has offered an excellent tool for long-term studies and was the method selected here for exploring the details of ebb-tidal delta morphology.

For measurement purposes, oblique time exposure images can be geo-rectified into horizontal maps such as Fig. 3 and converted to world coordinates using standard photogrammetry techniques (Holland et al., 1997). Projections were onto a horizontal surface located at an elevation determined by the tide level at each time of sampling. The resulting maps of image intensity, $\Psi(x, y, t)$, form the basis for subsequent analysis.

The domain of interest, as shown in Fig. 3, was selected as a region with both interesting meso-scale morphology and sufficient image resolution for follow-on analysis. The region spans 500 m on the cross-shore direction and 700 m on the alongshore. From the images, it is clear that the ebb-tidal delta is not continuous and smooth but is dissected into a large number of meso-scale features. From inspection of daily low tide images when depth-limited breaking was strongest it could be seen that these meso-scale features migrate in a clear pattern that will be the subject of later analysis.

4. Lag least squares analysis (LLSA) of migration rates

To calculate the migration rates of the bedform features from a sequence of daily time exposure images, an automated, objective method was developed based on a lag least squares analysis (LLSA) with the concept being as follows. If a feature in an image migrates at U m/day then it will be shifted in a later image by U times Δt where Δt is the time difference between the images. If the second image is sampled with that offset then the two images will look very similar. If we measure similarity by computing the variance over time for each pixel and summing over all the pixels, then the shift UΔt would yield a sum of squares deviation (represented here by χ) that has a smaller value than would be found for any other image shift. If U is unknown, a suite of possible values can be tested and the true value will be that for which χ is a minimum. In the current situation, two components of migration, U and V, are needed and the search is two-dimensional. For the case where multiple images are collected over a series of days, the variance is computed at each pixel over the full time series (and summed over all pixels). Because migration rates are expected to vary spatially, the analysis is done over a set of smaller sub-windows, or tiles, of the original image. The details of the analysis follow.

Within each rectified timex image ($\Psi(x, y, t)$), the analysis is carried out at a series of sub-windows, or tiles, with center locations (x_o, y_o) and tile sizes (dx, dy) such that the calculated sub-images (I) is:

$$I(x_o, y_o, t) = \Psi\left(x_o - \frac{dx}{2} : x_o + \frac{dx}{2},\ y_o - \frac{dy}{2} : y_o + \frac{dy}{2}, t\right). \quad (1)$$

To remove lighting variations, the intensities of the sub-images were normalized:

$$\hat{I} = \frac{I - \bar{I}}{\sigma_I} \quad (2)$$

where $\bar{I}$ and σ_I are the mean and standard deviation of intensities within the tile.

Initially, the suite of test velocities U and V were taken to range from −5 m/day to +5 m/day with a discretization, dU and dV of 0.25 m/day (i.e. test values of −5.00, −4.75, −4.50, …). However spurious values were sometimes found (i.e. where a feature in an early image matched a different feature in a much later image), so the search was narrowed and centered around seed guesses (U_o, V_o) previously calculated manually using the sequence of movie frames. The seed velocities were obtained for approximately 10 locations where the migration of the features was clear and highlighted by the wave dissipation over the shallow areas. The U_o and V_o were interpolated to the x_o and y_o locations, and then the U and V were obtained from:

$$U = [U_o - \Delta U : dU : U_o + \Delta U] \quad (3)$$

$$V = [V_o - \Delta V : dV : V_o + \Delta V] \quad (4)$$

where ΔU and ΔV are the span of plausible variation around the seed guesses, taken as ± 2 m/day.

From each available $\Delta t = t_i - t_1$, sub-images ($\hat{I}$) were stored in a stack (Ω) offset for the particular test values of U and V:

$$\Omega(U, V, \Delta t) = \hat{I}(x_o + U\Delta t, y_o + V\Delta t, \Delta t). \quad (5)$$

The sum of squared deviation ($\chi(U, V)$) was found by finding the variances through time at each pixel and summing them over the sub-image pixels:

$$\chi(U, V) = \sum(Var_t(\Omega)). \quad (6)$$

From the sum of squares deviation map ($\chi(U, V)$), the location of the minimum sum of squared deviation can be found and will correspond to the least squares estimate of migration rate, $\tilde{U}$ and $\tilde{V}$, respectively. If no minimum is found within the interior of the $\chi(U, V)$ domain (i.e. the minimum is on the border) no value is returned. The resolution of this method is limited by the choice of $dU = 0.25$ m/day. As a final step to improve accuracy, a paraboloid function (2D polynomial) was fit to the nine closest points in the neighborhood of $\tilde{U}$ and $\tilde{V}$:

$$\chi\left(\tilde{U} - \Delta U : \tilde{U} + \Delta U, \tilde{V} - \Delta V : \tilde{V} + \Delta V\right). \quad (7)$$

The paraboloid equation is described by:

$$Z = a_1 + a_2 U + a_3 U^2 + a_4 V + a_5 V^2. \quad (8)$$

The improved final estimates, denoted U_m and V_m, are found analytically as the minimum of the function. As a proxy for confidence intervals, σ_u and σ_v, for the migration rate estimates, we used the curvature terms of the paraboloid fit a_3 and a_5. While not a formal connection,

it is assumed that a large curvature will correspond to a well-defined minimum and a low curvature to a poorly defined one.

A total of 23 images spanning 22.8 days were selected for analysis, each corresponding to the lowest daylight tide of the day. The mean of the low tides was − 0.65 m ± 0.17 m. High tide images were discarded because of reduced breaking signatures. The regions around the shoreline including buildings and the dry beach area were masked out to remove their zero-velocity contribution to χ.

Results of the analysis showed some dependence on the size of each sub-window, reducing statistical stability for tiles that were too small but smearing spatial variability for tiles that were too large. After experimentation the best results were found when tiles were small in the onshore region ($x < 0$ m) and larger on the offshore region ($x > 0$ m), presumably due to the larger size of offshore features and the lower image resolution. The best size tested for offshore tiles was found to be dx = 100 m and dy = 200 m. In the onshore region, the sub-windows varied from dx = 30 m and dy = 60 m between in the region of smaller features to dx = 60 m and dy = 120 m where features were larger.

Migration rates were first found using the full available time series of 23 images, yielding mean rates based on all available information. However, the analysis could also be run on pairs of images to yield results that have better time resolution, for example allowing study of variability of migration rates over the sampling period. Typically these pair-wise estimates are noisier but can be averaged to reduce noise. In the discussion below these approaches will be termed the full stack and the pair-wise methods. It was quickly realized that the minimum time gap between image pairs was four days since the images resolution was 1 m, both in x and y directions, and the test velocities' discretization was 0.25 m/day. Thus a time span of less than four days meant that predicted image shifts could be less than 1 pixel.

5. Comparison between Argus and survey data

To determine the nature of the apparent bathymetric features seen in the time exposure images, they were compared to the surveys collected during the experiments. In Fig. 4 an example survey is compared with a geo-rectified timex image over the region of interest. From this figure, it can be seen that the Argus images provide a good qualitative visual proxy for the larger scale bathymetric features including breaking patterns on the main lobe of the ebb-tidal delta to the southwest and showing the offshore extent of the ebb-tidal delta, and an absence of breaking marking the locations of the main and secondary channels in the offshore delta.

The link between white dissipation features in time exposure images and underlying bathymetry has been demonstrated many times for open beach sand bars (e.g. Lippmann et al., 1993) but not for meso-scale ebb-tidal delta features. Fig. 5 shows an example comparison between raw survey data from one cross-shore survey transect and pixel intensities (timex image) over the same cross-shore transect (y = −540 m) extracted from and illustrated in Fig. 3 (white line). The main morphology features are well represented, for example the shoals at x = 40, 120 and 180 m and the correlation between the signals for the shoal region ($x < 225$) was $r = 0.35$. The persistence of the timex features also reinforces the bathymetric nature of the signals. It should be noted that comparisons of timex data directly with the gridded survey data in Fig. 4, would be misleading for shorter meso-scale features since the gridded data are highly smoothed, hence the use of raw data for the cross-shore transects. It should also be noted that correlations between bathymetry and timex intensity should not be perfect since wave breaking leads timex bright signals, for example, a high tide timex might show no breaking over the same bathymetry. Thus, low tide timex images do a good job revealing the location of shoal features but not the actual bathymetry.

6. Results

6.1. Bedform wavelength scales

Image intensity transects were extracted from the time exposure in Fig. 3 along both an example cross-shore (black line) and alongshore (white line) pixel transect. Fig. 6 is a raw, unsmoothed spectra of the both spatial transects (y = −540 m and x = −90 m). In the case of the cross-shore transect, almost all the variance is at length scales longer

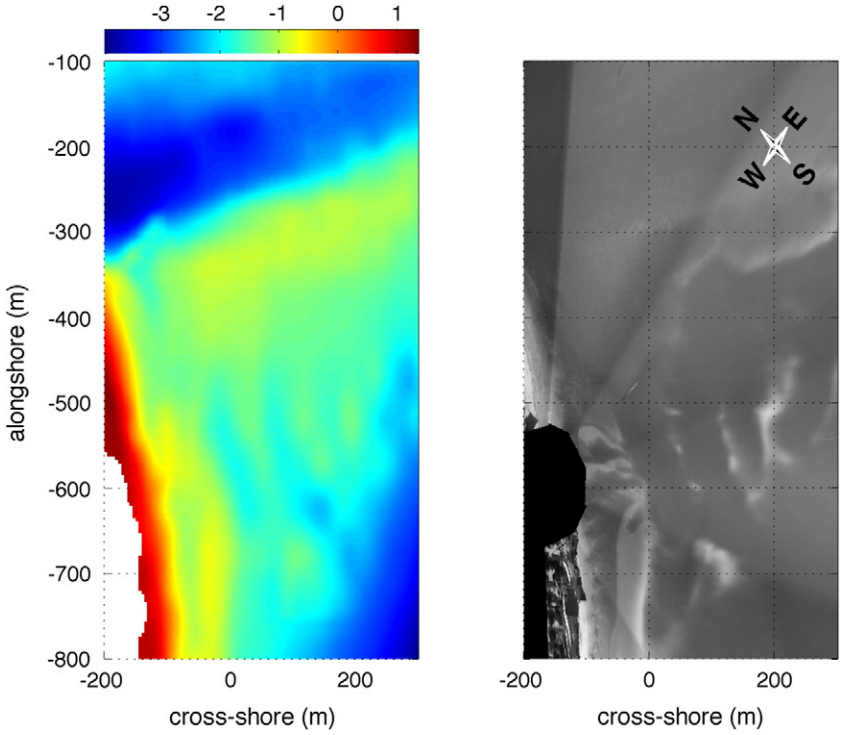

Fig. 4. Comparison between the survey for 05/10/2012 and Argus data over the area of interest, the southerly lobe of the ebb-tidal delta.

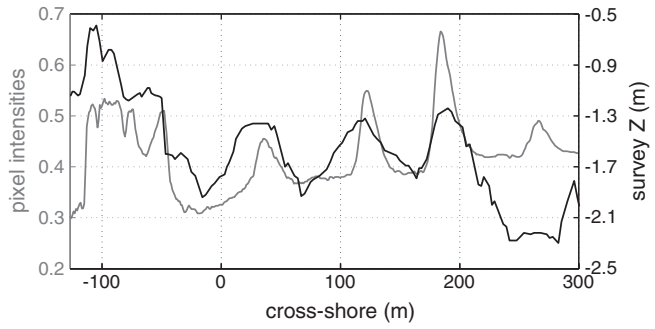

Fig. 5. Comparison between survey data (black line) and timex image (pixel intensities; gray line) over a cross-shore transect at the alongshore position y = −540 m (white line showed in Fig. 3).

than 20 m, but 55% lies in the band between 10 and 100 m. For the alongshore transect, 60% of the variance lies in the wavelengths between 10 and 100 m. Thus, these meso-scale morphologies are shorter than the larger-scale ebb-tidal delta lobe or the swash-bars along the shoreline, but much longer than megaripples (1–6 m).

6.2. Migration patterns

The 23 days of data collection allowed us to assess the spatial stability of these meso-scale features in the ebb-tidal delta. Much to our surprise, we found that these features were not only mobile, but migrated in a circular pattern with offshore features moving away from the ebb channel and toward the shore, and inshore features moving steadily back toward the channel. This is most apparent in video animations of the sequence of time exposures but can also be seen in time-space plots or timestacks which show a time dependence of pixel intensities along cross-shore or alongshore pixel transects. The video animation is available and accompanies the electronic version of this manuscript. To access this video simply click on the image below (online version only).

Fig. 7 shows eight image frames (each frame represents one day) during low tide. These frames were obtained from the video component to illustrate the migration of some bedform features, in this case, the small ones near the shoreline. In this figure, we observe a migration toward the inlet, and if we estimate a rate for this movement, we see that the meso-scale morphology (around y = −560) move around 30 m in 8 days. Fig. 8 shows timestack plots of cross-shore pixel intensities at two y-locations: y = −540 m and y = −700 m. In the left panel, the three white vertical bands correspond to the three shoals discussed in

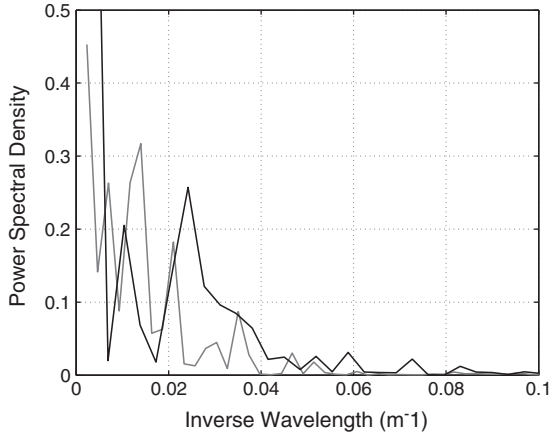

Fig. 6. Power spectra density to quantify the wavelength bands of energy of the shoals. The gray line is the cross-shore pixel transect at y = −540 m; the black line is the alongshore pixel transect around x = −90 m and x = −100 m. This last transect illustrated the existence of shorter scale morphologies along the shoreline.

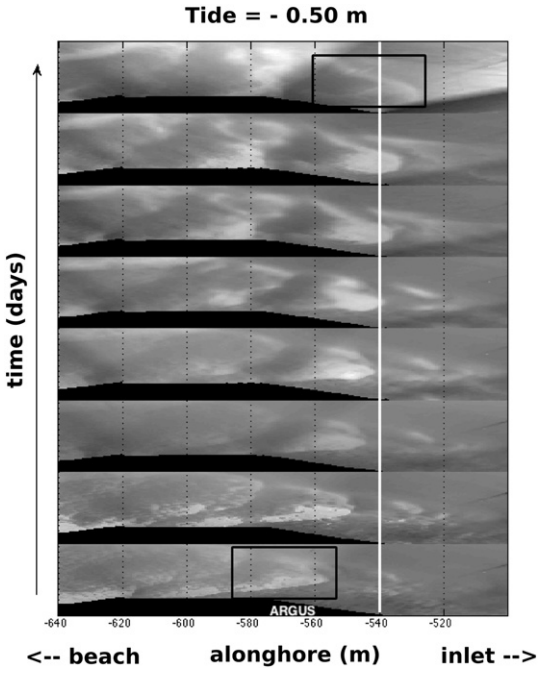

Fig. 7. Examples of 8 image frames (each image represents one day at low tide) obtained at NRI. The time proceeds from the bottom to top. The black rectangles enhance one of the bedform morphologies, illustrating the initial position and the end position, respectively. The inlet is at the right side of the figure. The white line indicated the position of the cross-shore transect at y = −540.

Fig. 5. The offshore features (x ~ 120 and 200 m) move (toward smaller x) as time progresses down the page indicating a shoreward migration with time. In contrast, the inshore features between − 100 m < x < 0 m, generally move to the right or toward the ebb-tidal delta. Right panel shows features generally migrating shoreward with time including the sandbar (larger scale feature) between − 100 m < x < 0 m. Rates of migration vary over the 23 days of data collection.

Both the results from these time-space plots and direct viewing of movie animations demonstrate a circular migration pattern for the meso-scale morphology features in this ebb-tidal delta. Offshore morphologies tend to migrate to the southwest, away from the ebb main channel, then move onshore, due to the wave-driven currents. Features near the shoreline migrate to the northeast, toward the inlet, due to the wave-driven longshore current and the flood flows on the marginal channels of the inlet. These observations are important to understanding the processes and magnitudes of sediment transport in ebb-tidal delta systems.

The migration rates calculated using the LLSA method for the full stack and pair-wise results averaged over the entire data set are shown in Fig. 9. Both methods yield essentially the same pattern, specifically a rotational circulation with meso-scale features on the offshore region going toward the shore and features in the inshore region migrating toward the inlet. Differences between the two methods were generally small with an average magnitude difference of 0.06 m/day. The main difference is related to the likelihood of successful data returns, particularly in the inshore region around − 600 m < y < −500 m. In this region, the morphology is dominated by short scale features and changes in migration rate through the full collection likely smeared minimum in the sum of squares deviation, yielding no result. In contrast, pair-wise estimates would yield a series of well-defined minima whose values could be averaged. For the pair-wise method, it was also calculated the migration rates for each tidal cycle, i.e., spring and neap, however it was not found a significant difference in the rates between these periods, probably due to the short data set (one spring-neap cycle).

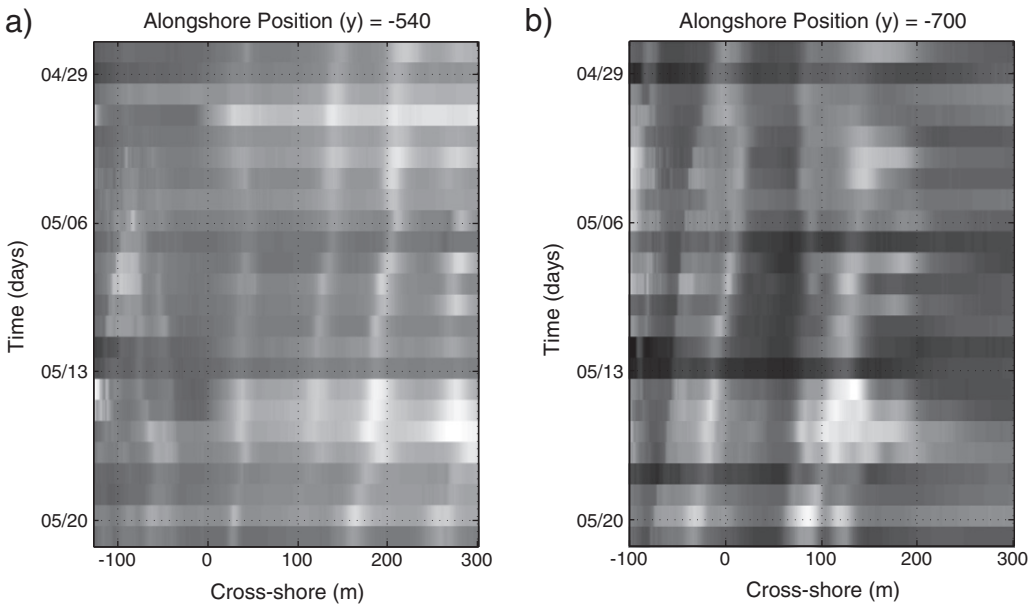

Fig. 8. Time-space plots of cross-shore vectors of pixel intensities at: (left) y = −540 and (right) y = −700 m. Time proceeds from the top to the bottom of the page. Movement of features down to the left corresponds to shoreward migration while down to the right indicates migration toward the ebb-tidal delta. Horizontal banding is caused by lighting fluctuations, for example sunny or cloudy days.

Since the pair-wise method reduces statistical noise by averaging a set of estimates, it is important to keep track of the number of successful estimates at each location. Therefore, it was calculated a map of percentages of good data (not shown) from the 23 days of data set. This revealed that most of the features in the region near the inlet returned a percentage of 20% of poor estimate of the velocities rates, and then, this value was chosen to be a threshold, and data with percentages less than this number were removed.

The map of the magnitudes of migration rates (not shown) revealed that the highest migration rates are associated with the meso-scales on the south-west side of the ebb-tidal delta (below y = -500 m). Rates are typically 2.0 to 3 m/day and in some places can reach 3.5 m/day. Migration rates nearer the inlet and in the region around x = 50 m are typically between 1.0 and 1.5 m/day. Fig. 10 is a histogram of the migration rate distribution. According to this figure, 72% of the rates exceed 1.0 m/day while 31% of the rates are greater than 2.0 m/day. The mean and standard deviation of migration rates is 1.53 and 0.76 m/day, respectively.

To better define the rotational pattern, the cross-shore averaged U-component and longshore average V-component as a function of the alongshore and cross-shore direction, respectively, were calculated and shown in Fig. 11. These are essentially the terms that define vorticity of the pattern. From Fig. 11 (upper panel), we note that cross-shore rates are primarily shoreward with decreasing magnitude toward the inlet. A weak positive (offshore) peak at y = −300 m is based on very few points, so it is not significant. Fig. 11 (lower panel), the alongshore average U-component, clearly shows the rotational nature of the pattern about a rotation center around x = 10 m with velocities directed

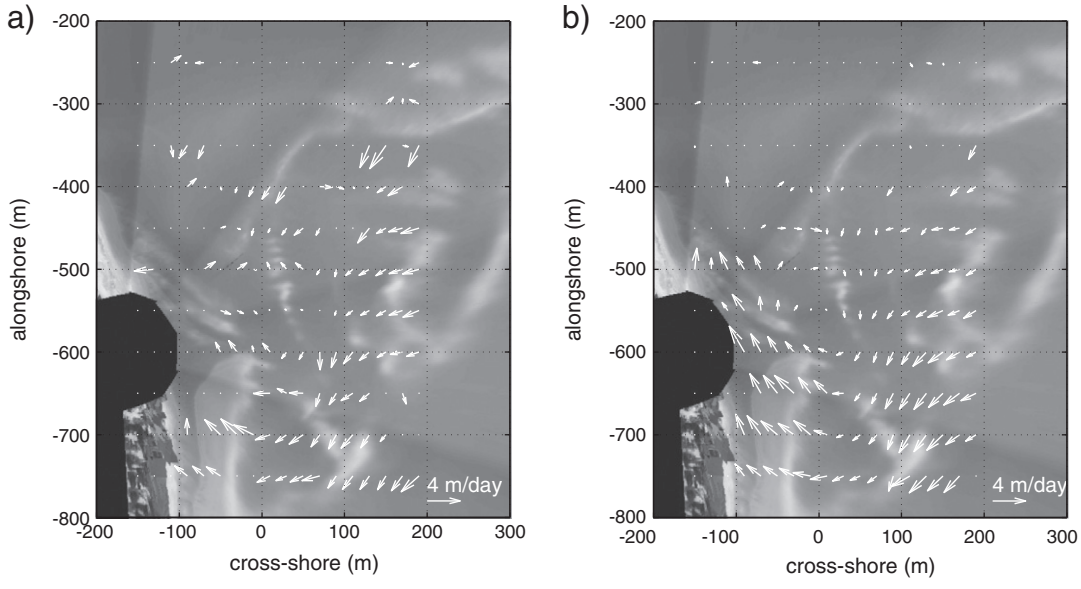

Fig. 9. Migration rates calculated using the full stack method (left) and pair-wise method (right).

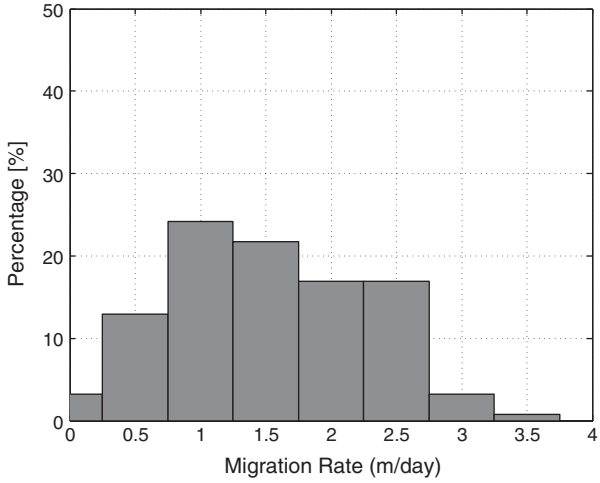

Fig. 10. Histogram of the migration rate magnitudes for the pair-wise method.

to north on the left side of this center, and directed to south on the right side. This rotation center is located approximately 110 m from the shoreline.

7. Discussion

The application of video imaging techniques has been used to describe and better understand the dynamics of meso-scale features associated with an ebb-tidal delta system. The behavior of swash bars, features with typical scales larger than 100 m, has been well documented (Oertel, 1972, 1975; Hine, 1975; Hubbard et al., 1979; FitzGerald, 1984; Smith and FitzGerald, 1994; Kana et al., 1999; Balouin et al., 2001, 2004; Robin et al., 2007, 2009; Son et al., 2010). However, our findings differ from prior publications in several ways. First, the focus is on what we have termed meso-scale morphologic features, with length scales between 10 and 100 m, shorter than scales typically reported previously. The ease and spatial resolution of the Argus method for visualizing morphology were key to detecting these scales and mapping them over time. Second, the migration rates have been found to be larger, i.e., they migrate quite quickly, which was not previously reported. We find that 72% of observed rates exceed 1.0 m/day. Third, the full time-space mapping of these features and development of a robust migration rate estimator have allowed us to produce full two-dimensional maps over a large area of an ebb-tidal delta lobe including identification of a center of rotation approximately 110 m from the shoreline.

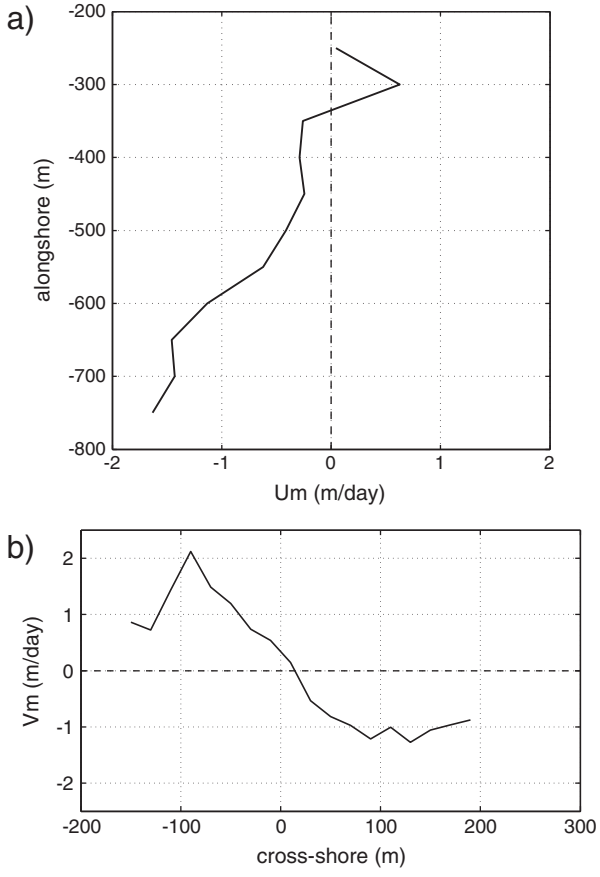

Fig. 11. The cross-shore averaged *U*-component as a function of the alongshore coordinate (upper) and the alongshore averaged *V*-component as a function of the cross-shore coordinate (lower).

At the New River Inlet, the observational data collected during the experiment, revealed that the main channel is ebb-dominated with strong outflow and located at the southwest side of the inlet, but there is also a secondary channel at the northeast side with a weak flow (e.g. Wargula et al., 2014). At the main channel, the flow is also subdivided in two sections, one over the ebb-tidal delta lobe and another directed seaward. Due to the centered flow in the main channel, the flood flow is dominant around the shallow areas and in the marginal channels generating a net flood directed flow, which transport sand onshore and into the inlet. However, due to the strong ebb flows in the main channel, the sand is not necessarily transported into the inlet, being recirculated back onto the ebb-tidal delta instead. This recirculation will be important since it can limit the sediment transfer between the inlet and the ebb-tidal delta. According to results obtained through numerical model simulated at NRI by Chen et al. (2012), the residual flow velocities present such patterns, especially when the waves are included in the simulations. Similar patterns were also observed by Elias and Hansen (2013)) at the San Francisco inlet through the use of numerical modeling. Thus, the sand transport by flood flow toward the inlet is, in part, restricted by the ebb jet and the sediments are recirculated back to the ebb-tidal delta, limiting the sediment bypass through into the inlet. Although the purpose of the present work is not to investigate the wave effects over the circulation pattern, it is important to mention their importance in increasing onshore flows in the shallow regions.

The formation of such gyres can have an important role for the sediment budget of the ebb-tidal delta system and the adjacent shorelines. Consequently, the meso-scale features have an important function as exchange mechanism of sediment between the ebb-tidal delta, the adjacent shoreline and the inlet. The understanding of how these features migrate and at which rate is essential for the estimate of the overall net sediment transport. Therefore, an interesting outcome here presented is that these features migrate at unexpected large rates, showing how dynamic and complex the system is and how quickly these exchanges can occur within the environment. Unfortunately, due to the relative short dataset, it was not possible to correlate these rates with the wave data. This is an aspect that needs further investigations.

Another important result from this study is the detection of the clear circular migration pattern of the meso-scales features (Fig. 11). The cross- and alongshore components, when combined, show the rotation of the features, in agreement with the residual flow velocities at NRI, as discussed above. The net longshore flow is downdrift toward the inlet over the inshore region, due to the flood directed flow on the shallow areas of the inlet. Over the offshore region, the longshore flow is toward southwest or away from the inlet. This circulation is completed by the net cross-shore flow. In main channel, due to the ebb currents, the transport is seawards, whereas on the other parts of the inlet outside the main channel, the transport of sand is onshore, due to all other current producing processes, such as waves and flood flow. The onshore

migration was also evidenced by the large swash bar near the shoreline which was also about to attach to the beach, during the experiment.

Despite the fact that the features are moving, it is important to comment that it is not always true to infer that all the sand comprised on the morphologies will keep the same form as it migrates. Some sand will move independently of the bedform. This was particularly noted on the meso-scale features located in the inshore regions. While the observation that morphology migrates in a circular pattern would seem to imply a similar pattern of sediment transport, this is not necessarily true. Morphologic changes depend only on gradients in sediment transport, not the actual values. For example, river bedform can be found to migrate upstream under the right conditions even though sediment transport is clearly downstream (Kennedy, 1969; Engelund and Fredsoe, 1982; Fredsoe, 1986). Nevertheless, as is often done with oscillatory bottom ripples, it is tempting to estimate the transport as the product of the volume of the migrating form times its migration rate divided by the time for passage. If we take the typical height of an offshore feature to be 0.15 m and the length 80 m (Fig. 5) and if the migration rate is taken to be 2.0 m/day, the resulting transport will be 0.3 m^3/day.

The results obtained here were based on only 23 days of data, the duration of Argus collections for this specific field experiment. However, once installed, an Argus station can continuously collect data at low cost and much longer records could be collected. With a longer data set, the dependence of migration rates and patterns on wave conditions can be calculated. While the introduction of sediment transport modeling based on these data is well beyond the scope of this paper, it would provide a good focus for future work.

8. Conclusions

Timex exposure images of wave breaking patterns allow the low-cost measurement of morphological patterns in an ebb-tidal delta environment. When applied at the New River Inlet in 2012, we found that the ebb-tidal delta was primarily composed of a complex pattern of meso-scale features with scales that are less than 100 m but are longer than megaripples. Therefore, due to spatial resolution limitations, it would be very difficult to measure such features using traditional surveying methods. Based on two typical transects, 60% of the variance lies in the band between 10 and 100 m length scales.

When viewed as a movie sequence of time exposures collected over the 23 days of a 2012 field experiment at New River Inlet, NC, it was clear that the meso-scale features were circulating in a clockwise sense with movement in offshore regions being away from the inlet mouth while nearshore migration was back toward the inlet. To quantify migration rates and patterns objectively based on sequences of time exposure images, a Lagged Least Squares Algorithm (LLSA) was developed that found the vector migration rate for which the suite of lagged images were most similar, computed on a tile-by-tile basis.

This analysis revealed a very clear and dynamic circulation observed between the meso-scale morphologies around the ebb-tidal delta. This circular pattern of migration appears consistent with the expected residual flow velocities an ebb-delta system, with a strong ebb flow concentrated at the main channel which generates a seaward transport, whereas on the regions outside the main channel, the net sediment transport is onshore (due to wave-driven currents and flood flow). Over the adjacent shallow areas of the inlet, there is a net flood directed flow toward the inlet. On this flood flow, the transfer of sand into the inlet can be limited by the strong ebb jet and the sand may recirculate back to the ebb-tidal delta, completing the circular pattern.

The circulation is similar to migration patterns previously observed for swash bars migrating landward, but the scales of the features are clearly smaller, the sampling is spatially and temporally more dense and the migration rates from LLSA are much larger. The mean migration rate was found to be 1.53 m/day (standard deviation of 0.76 m/day). 72% of estimated rates were greater than 1.0 m/day and 31% were larger than 2.0 m/day. The maximum rate found was 3.5 m/day, averaged over 23 days. Alongshore averages of cross-shore migration rates show that a node occurs at 110 m from the shoreline that separates migration away from the inlet from migration toward the inlet near the shore. Therefore, the importance of the shorter length scales of the observed meso-scale features and the higher observed migration rates that was not previously reported in the literature deserve further study, since these features seem to be important for the exchange of sediments between the ebb-tidal delta, the shoreline and the inlet, i.e., for the sediment budget of the system.

Because time exposure methods can be used for long duration at low cost, they would be very useful in future longer studies that would allow measurement of the influence of variations of wave conditions and tidal range in ebb-tidal delta dynamics.

Supplementary data to this article can be found online at http://dx.doi.org/10.1016/j.margeo.2014.09.045.

Acknowledgments

The Coastal Imaging Laboratory from Oregon State University participated in the DARLA program (Data Assimilation and Remote-Sensing for Littoral Applications) with support from the Office of Naval Research, grant number N000141010932. We appreciate the use of AWAC data, provided by Steve Elgar and Britt Raubenheimer and help with surveying and other instrumentation issues from Dan Clark, Tom Lippmann and Chris Chickadel. We thank Adam Keen for Argus field support. Survey data was collected by the Jesse McNinch and the team from the Field Research Facility (FRF). The Coastal Data Information Program (CDIP) for the waverider buoy data. As usual, none of this would have happened without the help of John Stanley. Support for Cassia Pianca was provided by São Paulo Research Foundation (FAPESP — 2010/13083-3). Eduardo Siegle is sponsored by a CNPq research fellowship. We would like to thank the two anonymous reviewers for their suggestions and comments.

References

Balouin, Y., Howa, H., Michel, D., 2001. Swash platform morphology in the ebb-tidal delta of the Barra Nova inlet, South Portugal. Journal of Coastal Research 17, 784–791.
Balouin, Y., Morris, B., Davidson, M., Howa, H., 2004. Morphology evolution of an ebb-tidal delta following a storm perturbation: assessments from remote sensed video data and direct surveys. Journal of Coastal Research 20, 415–423.
Bruun, P., Gerritsen, F., 1960. Stability of Coastal Inlets. North-Holland Publishing Company, Amsterdam.
Cayocca, F., 2001. Long-term morphological modeling of a tidal inlet: the Arcachon Basin, France. Coastal Engineering 42, 115–142.
Chen, J., Hsu, T., Shi, F., 2012. Numerical modeling of hydrodynamics and sediment transport of new river inlet (nc) using NearCoM-TVD, Ocean Science Meeting, Session 29. Nearshore Processes B0822.
Cleary, W., Hosier, P., 1987. Onslow beach n.c.: morphology and stratigraphy. In: Kraus, N.C. (Ed.), Coastal Sediments 87. American Society of Civil Engineers, pp. 1745–1759.
Cleary, W., Wilson, K., Jackson, C., 2006. Shoreline restoration in high hazard zones: Southeastern North Carolina, USA. Journal of Coastal Research, SI 884–889.
Dean, R., Walton, T., 1975. Sediment transport processes in the vicinity of inlets with special reference to sand trapping. Estuarine Research, pp. 3–22.
Elias, E., Hansen, J., 2013. Understanding processes controlling sediment transports at the mouth of a highly energetic inlet system (San Francisco Bay, CA). Marine Geology 345, 207–220.
Elias, E., Spek, A., 2006. Long-term morphodynamic evolution of texel inlet and its ebb-tidal delta (The Netherlands). Marine Geology 225, 5–21.
Engelund, F., Fredsoe, J., 1982. Sediment ripples and dunes. Annual Review of Fluid Mechanics 14, 13–37.
FitzGerald, D., 1984. Interactions between the ebb-tidal delta and landward shoreline: Price Inlet, South Carolina. Journal of Sedimentary Petrology 54, 1303–1318.
FitzGerald, D., Kraus, N., Hands, E., 2000. Natural mechanisms of sediment bypassing at tidal inlets. Technical Report CHETN-IV-30. Army Corps of Engineers, Vicksburg, MS, US.
FitzGerald, D., Buynevich, I., Hein, C., 2012. Morphodynamics and Facies Architecture of Tidal Inlets and Tidal Deltas, 301–333.
Fredsoe, J., 1986. Physics of desertification. Chapter Formation of Ripples, Dunes, and Antidunes in River Beds. Springer Netherlands, pp. 327–343.
Hayes, M., 1975. Morphology of sand accumulations in estuaries: an introduction to the symposium. Estuarine Research, pp. 3–22.
Hayes, M., Goldsmith, V., Hobb, C., 1970. Offset coastal inlets. 12th Coastal Engineering Conference. Amer. Soc. Civil Engrs, pp. 1187–1200.

Hine, A., 1975. Bedform distribution and migration pattern on tidal deltas in the Chatman Harbor Estuary, Cape Cod, Massachusetts. Estuarine Research, pp. 3–22.
Holland, K., 1998. Beach cusp formation and spacings at duck, usa. Continental Shelf Research 18, 1081–1098.
Holland, K., Holman, R., Lippmann, T., Stanley, J., Plant, N., 1997. Practical use of video imagery in nearshore oceanographic field studies. IEEE Journal of Oceanic Engineering 22, 81–92.
Holman, R., Stanley, J., 2007. The history and technical capabilities of Argus. Coastal Engineering 54, 477–491.
Holman, R.A., Sallenger, A.H., Lippmann, T.C., Haines, J.W., 1993. The application of video image processing to the study of nearshore processes. Oceanography 6, 78–85.
Hubbard, D.K., Oertel, G., Nummedal, D., 1979. The role of waves and tidal currents in the development of tidal-inlet sedimentary structures and sand body geometry: examples from North Carolina, South Carolina, and Georgia. Journal of Sedimentary Research 49.
Kana, T.W., Hayter, E.J., Work, P.A., 1999. Mesoscale sediment transport at southeastern U.S. tidal inlet: conceptual model applicable to mixed energy settings. Journal of Coastal Research 15.
Kennedy, J.F., 1969. The formation of sediment ripples, dunes, and antidunes. Annual Review of Fluid Mechanics 1.
Komar, P.D., 1996. Tidal-inlet processes and morphology related to the transport of sediments. Journal of Coastal Research, SI 23–45.
Lippman, T.C., Irish, J.D., Hunt, J., 2013. Subtidal flow structure in tidally modulated inlets. Coastal Dynamics, pp. 1095–1104.
Lippmann, T., Holman, R., 1989. Quantification of sand bar morphology: a video technique based on wave dissipation. Journal of Geophysical Research, Oceans 94, 995–1011.
Lippmann, T.C., Holman, R.A., Hathaway, K.K., 1993. Episodic, nonstationary behavior of a double bar system at Duck, North Carolina, U.S.A.,1986–1991. Journal of Coastal Research 15, 49–75.
Medina, R., Marino-Tapia, I., Osorio, A., Davidson, M., Martin, F., 2007. Management of dynamic navigational channels using video techniques. Coastal Engineering 54, 523–537.
Morris, B., Davidson, M., Huntley, D., 2001. Measurements of the response of a coastal inlet using video monitoring techniques. Marine Geology 175, 251–272.
Morris, B.D., Coco, G., Bryan, K.R., Turner, I.L., 2007. Video-derived mapping of estuarine evolution. Journal of Coastal Research 50, 410–414.
O'brien, M., 1931. Estuary tidal prisms related to entrance area. Journal of Civil Engineering 738–739.
Oertel, G.F., 1972. Sediment transport of estuary entrance shoals and the formation of swash platforms. Journal of Sedimentary Research 42.
Oertel, G.F., 1975. Ebb-tidal deltas of Georgia estuaries. Estuarine Research.
Pearre, N., Puleo, J., 2009. Quantifying seasonal shoreline variability at Rehoboth Beach, Delaware, using automated imaging techniques. Journal of Coastal Research 25, 900–914.
Plant, N.G., Aarninkhof, S.G.J., Turner, I.L., Kingston, K.S., 2007. The performance of shoreline detection models applied to video imagery. Journal of Coastal Research 23.
Ranasinghe, R., Pattiaratchi, C., 2003. The seasonal closure of tidal inlets: causes ans effectes. Coastal Engineering Journal 45, 601–627.
Robin, N., Levoy, F., Monfort, O., 2007. Bar morphodynamic behaviour on the ebb delta of a macrotidal inlet (Normandy, France). Journal of Coastal Research 23, 1370–1378.
Robin, N., Levoy, F., Monfort, O., 2009. Short term morphodynamics of an intertidal bar on megatidal ebb delta. Marine Geology 260, 102–120.
Shi, F., Hanes, D., Kirby, J., Erikson, L., Barnard, P., Eshleman, J., 2011. Pressure-gradient-driven nearshore circulation on a beach influenced by a large inlet tidal shoal system. Journal of Geophysical Research 116.
Siegle, E., Huntley, D., Davidson, M., 2004. Physical controls on the dynamics of inlet sandbar systems. Ocean Dynamics 54.
Siegle, E., Huntley, D., Davidson, M., 2007. Coupling video imaging and numerical modelling for the study of inlet morphodynamics. Marine Geology 236, 143–163.
Smith, J.B., FitzGerald, D.M., 1994. Sediment transport patterns at the Essex River inlet ebb-tidal delta, Massachusetts, U.S.A. Journal of Coastal Research 10, 752–774.
Son, C., Flemming, B., Bartholoma, A., 2010. Evidence for sediment recirculation on an ebb-tidal delta of the East Frisian barrier-island system, Southern North Sea. Geo-Marine Letters 31, 87–100.
Stive, M.J., Rakhorst, R.D., 2008. Review of empirical relationships between inlet cross-section and tidal prism. Journal of Water Resources and Environmental Engineering 23.
Van der Vegt, M., Schuttelaars, H., Swart, H., 2006. Modeling the equilibrium of tide-dominated ebb-tidal deltas. Journal of Geophysical Research 111.
Van Enckevort, I., Ruessink, B., 2003a. Video observations of nearshore bar behaviour. Part 1: alongshore uniform variability. Continental Shelf Research 23, 501–512.
Van Enckevort, I., Ruessink, B., 2003b. Video observations of nearshore bar behaviour. Part 2: alongshore non-uniform variability. Continental Shelf Research 23, 513–532.
Van Leeuwen, S.M., Van der Vegt, M., Swart, H.E., 2003. Morphodynamics of ebb-tidal deltas: a model approach. Estuarine, Coastal and Shelf Science 57.
Wang, Z.B., Louters, T., de Vriend, H.J., 1995. Morphodynamic modelling for a tidal inlet in the Wadden Sea. Marine Geology 126, 289–300.
Wargula, A., Raubenheimer, B., Elgar, S., 2013. The effects of wave forcing on circulation at New River Inlet, Nc. Coastal, Dynamics, pp. 1871–1880.
Wargula, A., Raubenheimer, B., Elgar, S., 2014. Wave-driven along- channel subtidal flows in a well-mixed ocean inlet. Journal of Geophysical Research, Oceans 119, 2987–3001.
Woodroffe, C.D., 2002. Coasts: Form, Process and Evolution. Cambridge University Press, Cambridge, UK; New York.